Hindawi
Mathematical Problems in Engineering
Volume 2018, Article ID 7627326, 11 pages
https://doi.org/10.1155/2018/7627326

Research Article

Analysis and Structure Optimization of Radial Halbach Permanent Magnet Couplings for Deep Sea Robots

Bo Cheng [1,2] **and Guang Pan** [1,2]

[1] *School of Marine Science and Technology, Northwestern Polytechnical University, Xi'an 710072, China*
[2] *Key Laboratory for Unmanned Underwater Vehicle, Northwestern Polytechnical University, Xi'an 710072, China*

Correspondence should be addressed to Guang Pan; panguang@nwpu.edu.cn

Received 5 April 2018; Accepted 27 August 2018; Published 12 September 2018

Academic Editor: Yannis Dimakopoulos

Copyright © 2018 Bo Cheng and Guang Pan. This is an open access article distributed under the Creative Commons Attribution License, which permits unrestricted use, distribution, and reproduction in any medium, provided the original work is properly cited.

Permanent magnet couplings (PMCs) can convert the dynamic seal of transmission shaft into a static seal, which will significantly improve the transmission efficiency and reliability. Therefore, the radial Halbach PMC in this paper is suitable as the transmission mechanism of deep sea robots. A two-segment Halbach array is adopted in the radial PMC, and the segment arc coefficient can be adjustable. This paper presents the general analytical solutions of the distinctive Halbach PMCs based on scalar magnetic potential and Maxwell stress tensor. The analytical solutions of magnetic field are in good agreement with 2-D finite element analysis (FEA) results. In addition, an initial prototype of the radial Halbach PMC has been fabricated, and the analytical solutions of magnetic torque are compared with 3-D FEA and experiment results. This paper also establishes an optimization procedure for PMCs based on the combination of 3-D FEA, Back Propagation Neural Network (BPNN), and Genetic Algorithm (GA). 3-D FEA is performed to calculate the pull-out torque of the samples from Latin hypercube sampling, then BPNN is used to describe the relationship between the optimization variables and pull-out torque. Finally, GA is applied to solve the optimization problem, and the optimized scheme is proved to be more reasonable with the FEA method.

1. Introduction

Deep sea robots have attracted more and more attention with the development of ocean explorations. However, as the submerged distance of deep sea robots increases, the dynamic seal problem of transmission shaft appears, especially in the propulsion system and joint of deep sea robots. The traditional dynamic seal will bring large friction loss, when working in larger submerged distance. Moreover, the reliability of traditional seal is still a problem, with the increase of operating time. The radial Halbach permanent magnet coupling (PMC) in this research can convert the rotationally dynamic seal of transmission shaft into a static seal and will significantly improve the sealing effect and reliability. Therefore, the research of PMCs is of great significance to enhance the dynamic performance of deep sea robots.

The schematic of the radial PMC for deep sea robots is shown in Figure 1. The inner and outer permanent magnets (PMs) are, respectively, fixed on the inner and outer rotor core. The inner rotor core is integrated with driving shaft, and the outer rotor core is integrated with driven shaft. The outer side of the isolation sleeve is seawater, and the inside is filled with oil to balance the pressure of the external seawater. To avoid eddy current loss, the isolation sleeve is made of nonconductive or high resistivity materials, such as high strength engineering plastics or ceramics.

The analytical methods of PMC analysis are based on the analysis of forces between two magnets [1–8] or based on the analysis of magnetic field [9–12]. The calculated results of the analytical methods were compared with the experimental or finite element analysis (FEA) results. Reference [13] designed and constructed an easy-to-use test-rig for static performance test of PMCs, and the coupling-performance shows a clear influence of end-effects for axially short couplings. H. B. Kang and J. Y. Choi et al. [14] presented a comparative study of torque analysis for synchronous PMCs with parallel- and conventional Halbach-magnetized magnets, using analytical field calculations based on the magnetic vector potential

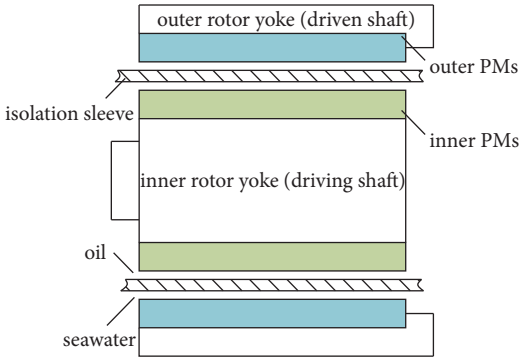

Figure 1: Schematic of the radial PMC.

and Maxwell stress tensor. In this paper, a two-segment Halbach array is adopted in the radial PMC. Different from the conventional Halbach, the segment arc coefficient can be adjusted. On the basis of scalar magnetic potential and Maxwell stress tensor, the general analytical solutions of radial Halbach PMCs are presented. An initial PMC prototype has been fabricated, and the analytical solutions of the prototype are compared with the FEA calculated and experimental results.

Although the analytical solution is very useful in analyzing the PMC parameters, analytical methods and 2-D FEA are proved to be not accurate enough, due to ignoring the end magnetic flux leakage effect. The structure optimization of PMCs should be based on 3-D FEA or experimental results. Reference [15] implemented an optimizing strategy consisting of the 3-D FEA, the design of experiments (DOE), and an exhaust algorithm in a small range to obtain the near-optimal parameter set of PMCs. W. Wu et al. [16] demonstrated the optimization process of PMCs using 3-D finite element methods combined with computer search techniques; this optimization process depends mostly on the initial feasible design and ignores the weight factor of design variables and their interaction with each other. Moreover, frequently used optimization procedures cannot be well integrated in experiments or 3-D FEA. Therefore, this paper presents a new optimization procedure for PMCs based on the combination of 3-D FEA, Back Propagation Neural Network (BPNN), and Genetic Algorithm (GA). An objective function is proposed to evaluate the mixed goal of maximal pull-out torque and minimal PM material mass. The BPNN prediction model of pull-out torque is established and proved to be relatively accurate. GA is applied to find the optimized scheme of the radial Halbach PMC, and the performance of the optimized scheme is compared with that of the initial design with the 2-D and 3-D FEA methods.

2. Radial Halbach PMC Analysis

2.1. Structure and Analytical Model. The cross section of the radial Halbach PMC in this paper is shown in Figure 2. The inner and outer PMs are, respectively, fixed on the inner and outer rotor core with high permeability, and the rotor cores will contribute to reducing the loss of flux. Due to

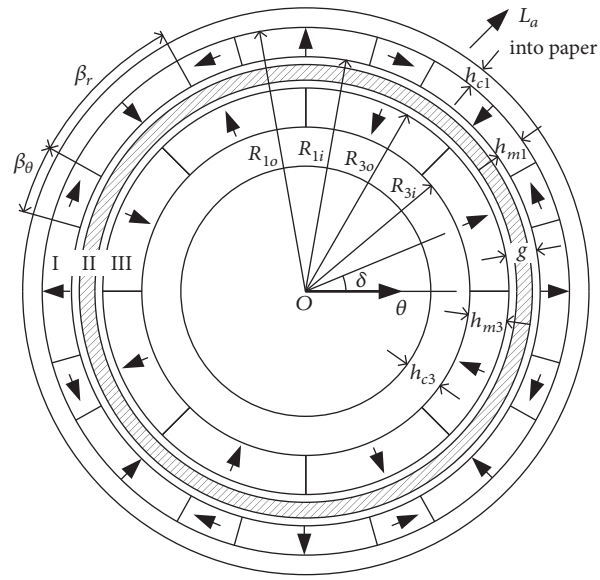

Figure 2: The cross section and analytical model of the radial Halbach PMC.

the space limitations of the transmission mechanism, the external dimensions of the radial PMC will be constrained, so the outer rotor is expected to be as thin as possible. In addition, the air gap between inner and outer magnets should be large enough, so that it can allow an isolation sleeve with sufficient thickness. Therefore, a two-segment Halbach array is adopted in the outer PMs, and the segment arc coefficient is adjustable. The segment arc coefficient represents the ratio of the arc of a radially magnetized segment β_r to the arc of a magnet pole β_p and is defined as follows:

$$\alpha_{rp} = \frac{\beta_r}{\beta_p} = \frac{\beta_r}{\beta_r + \beta_\theta} = \frac{\beta_r}{\pi/p} \tag{1}$$

where p stands for the pole pair number. In particular, when the segment arc coefficient is 0.5, the outer PMs will be a conventional Halbach array.

In addition, the internal space of the radial PMC is relatively sufficient, so the inner core and the inner PMs can be designed to be thick, and the inner PMs adopt the ordinary tile-shaped.

The magnetic torque between inner and outer PMs is an important indicator to evaluate the performance of PMCs, and it represents the ability of PMCs to transmit torque. Based on the analytical method of magnetic field, the magnetic torque is calculated and analyzed as follows.

2.2. Magnetic Field and Magnetic Torque. In order to obtain the PMC analytical solution, we assume that rotor cores are infinitely permeable, and the end-effects are neglected. In Figure 2, the analytical model is divided into three regions, in which regions I and III are the PMs and region II is air. In the polar coordinates, the radial magnetization of the Halbach array outer PMs is an even function, and the tangential

magnetization is an odd function, and the magnetization vector $\mathbf{M_1}$ can be given by

$$\begin{aligned}\mathbf{M_1} &= M_{1r}\mathbf{r} + M_{1\theta}\boldsymbol{\theta} \\ &= \sum_{n=1,3,5\cdots}^{\infty} M_{1rn}\cos(np\theta)\,\mathbf{r} \\ &\quad + \sum_{n=1,3,5\cdots}^{\infty} M_{1\theta n}\sin(np\theta)\,\boldsymbol{\theta}\end{aligned} \tag{2}$$

where

$$\begin{aligned}M_{1rn} &= \frac{4B_r}{\mu_0 n\pi}\sin\left(\frac{n\pi\alpha_{rp}}{2}\right), \\ M_{1\theta n} &= \frac{4B_r}{\mu_0 n\pi}\cos\left(\frac{n\pi\alpha_{rp}}{2}\right).\end{aligned} \tag{3}$$

When the relative angular displacement between the inner and outer PMs is δ, the magnetization vector $\mathbf{M_3}$ of the inner PMs can be written as follows:

$$\mathbf{M_3} = M_{3r}\mathbf{r} + M_{3\theta}\boldsymbol{\theta} = \sum_{n=1,3,5\cdots}^{\infty} M_{3rn}\cos\left[np\left(\theta-\delta\right)\right]\mathbf{r} \tag{4}$$

where

$$M_{3rn} = \frac{4B_r}{\mu_0 n\pi}\sin\left(\frac{n\pi\alpha}{2}\right). \tag{5}$$

The magnetic flux density vectors $\mathbf{B_{1,3}}$ in the PM region and $\mathbf{B_2}$ in the air regions can be expressed as follows:

$$\begin{aligned}\mathbf{B_{1,3}} &= \mu_0\mu_r\mathbf{H_{1,3}} + \mu_0\mathbf{M_{1,3}} \\ \mathbf{B_2} &= \mu_0\mathbf{H_2}\end{aligned} \tag{6}$$

where μ_r is the relative permeability, $\mathbf{H}$=-grad φ, and φ is the scalar magnetic potential.

The scalar magnetic potential in the PM regions can be governed by quasi-Poissonian equations, while, in air region, it can be governed by Laplace's equation. The magnetic field produced by the Halbach array PMs is described by the scalar magnetic potential, as shown in

$$\begin{aligned}\nabla^2\varphi_1 &= \frac{\partial^2\varphi_1}{\partial r^2} + \frac{1}{r}\frac{\partial\varphi_1}{\partial r} + \frac{1}{r^2}\frac{\partial^2\varphi_1}{\partial\theta^2} = \frac{1}{\mu_r}\operatorname{div}\mathbf{M_1} \\ \nabla^2\varphi_2 &= \frac{\partial^2\varphi_2}{\partial r^2} + \frac{1}{r}\frac{\partial\varphi_2}{\partial r} + \frac{1}{r^2}\frac{\partial^2\varphi_2}{\partial\theta^2} = 0 \\ \nabla^2\varphi_3 &= \frac{\partial^2\varphi_3}{\partial r^2} + \frac{1}{r}\frac{\partial\varphi_3}{\partial r} + \frac{1}{r^2}\frac{\partial^2\varphi_3}{\partial\theta^2} = \frac{1}{\mu_r}\operatorname{div}\mathbf{M_3}\end{aligned} \tag{7}$$

The general solutions of the scalar magnetic potential in the PMs and air regions are given by the following:

$$\begin{aligned}\varphi_1(r,\theta) &= \sum_{n=1,3,5\cdots}^{\infty}\left(a_{1n}r^{np} + b_{1n}r^{-np}\right)\cos(np\theta) \\ &\quad + \sum_{n=1,3,5\cdots}^{\infty}\frac{M_{1rn} + npM_{1\theta n}}{\mu_r\left[1-(np)^2\right]}r\cos(np\theta)\end{aligned} \tag{8}$$

$$\varphi_2(r,\theta) = \sum_{n=1,3,5\cdots}^{\infty}\left(a_{n2}r^{np} + b_{n2}r^{-np}\right)\cos(np\theta) \tag{9}$$

$$\begin{aligned}\varphi_3(r,\theta) &= \sum_{n=1,3,5\cdots}^{\infty}\left(a_{n3}r^{np} + b_{n3}r^{-np}\right)\cos(np\theta) \\ &\quad + \sum_{n=1,3,5\cdots}^{\infty}\frac{M_{r3n}}{\mu_r\left[1-(np)^2\right]}r\cos\left[np\left(\theta-\delta\right)\right]\end{aligned} \tag{10}$$

where $np\neq 1$.

The boundary conditions to be satisfied are shown as follows:

$$\begin{aligned}H_{1\theta}\big|_{r=R_{1o}} &= 0 \\ H_{3\theta}\big|_{r=R_{3i}} &= 0 \\ H_{1\theta}\big|_{r=R_{1i}} &= H_{2\theta}\big|_{r=R_{1i}} \\ B_{1r}\big|_{r=R_{1i}} &= B_{2r}\big|_{r=R_{1i}} \\ H_{2\theta}\big|_{r=R_{3o}} &= H_{3\theta}\big|_{r=R_{3o}} \\ B_{2r}\big|_{r=R_{3o}} &= B_{3r}\big|_{r=R_{3o}}\end{aligned} \tag{11}$$

The tangential force between the inner and outer PMs can be derived by the Maxwell stress tensor, and the magnetic torque of PMCs is produced by the tangential force. If the tangential force is integrated along a circle of radius r in air region II, the magnetic torque of the radial Halbach PMC can be expressed as follows:

$$T_m = \frac{L_a}{\mu_0}\oint r^2 B_{2r}B_{2\theta}\,d\theta \tag{12}$$

3. Comparison with FEA and Experiment

3.1. Magnetic Field. The initial design of the radial PMC adopts a conventional Halbach array with equal segment, and the initial design parameters are shown in Table 1. The computational domain diameter of the 2-D and 3-D FEA model is 1.2 times that of the radial Halbach PMC. The 2-D FEA results of the PMC magnetic field distributions in different relative angular displacements are illustrated in Figure 3.

Figure 4 shows the comparison between the analytical solutions and 2-D FEA results of radial and circumferential flux density in air region, when δ is 0°, 15°, and 30°. We can see that the analytical solutions of flux density in air region under different relative angular displacement are in good agreement with the 2-D FEA results.

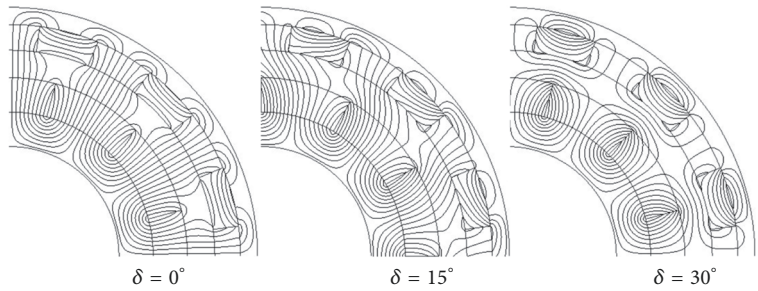

Figure 3: Magnetic field distributions from 2-D FEA.

Table 1: Initial design parameters of the radial Halbach PMC.

Parameters	Value
Axial length L_a	50mm
Outer radius of outer PMs R_{1o}	27mm
Inter radius of outer PMs R_{1i}	24mm
Outer radius of inner PMs R_{3o}	20.8mm
Inter radius of inner PMs R_{3i}	16.8mm
Pole pair number p	6
Segment arc coefficient α_{rp}	0.5
Pole-arc coefficient α	1
Remanence B_r	1.39T
Relative permeability μ_r	1.03
Rotor core material	Steel_1010
Outer rotor core thickness h_{c1}	2mm
Inner rotor core thickness h_{c3}	4mm

3.2. Magnetic Torque. Figure 5 shows the experimental apparatus for measuring the PMC magnetic torque. It mainly consists of the PMC prototype, a torque sensor, and a stepping motor to rotate the PMC inner rotor. The step angle of the stepping motors is 1.5°. The maximal positioning error is 3%, and the stepping motor has no cumulative error precision. The measurement error of the torque sensor is ±0.5%. As can be seen from Figure 5, the PMC outer rotor is fixed on the torque sensor and is supported by bearings. During the experiment, the PMC outer rotor is not rotated. When the PMC inner rotor rotates to a certain angle, the corresponding magnetic torque can be measured by the torque sensor.

3-D FEA are also used to calculate the PMC magnetic torque in this paper. The magnetic torque from the analytical solution, 3-D FEA, and experiments with changes of the relative angular displacement are shown in Figure 6. When the inner and outer PMs are aligned, the PMC is at the zero torque position, and when the angular displacement is 15° mechanical degree, the magnetic torque reaches its peak. As the relative angular displacement further increases, the magnetic torque will decrease to zero at 30° mechanical degree. Therefore, the maximal magnetic torque is also called pull-out torque T_{max}, which reflects the maximal ability of PMCs to transmit torque.

Table 2: Comparison with experimental pull-out torque.

Analytical solution (error)	3-D FEA (error)	Experiment
25.9N·m (11.6%)	23.6N·m (1.7%)	23.2N·m

The analytical solution and 3-D FEA results of pull-out torque are compared with the experimental results, as shown in Table 2. We can see that the pull-out torque calculated with the analytical method is 11.6% larger than the experimental result; by contrast, 3-D FEA result is close to the experimental result. This is due to the assumptions of the analytical model for simplifying calculation, and the analytical solution ignores the end magnetic flux leakage effects. Despite consuming more computing resources and time, 3-D FEA has higher simulation accuracy.

In this research, considering the transmitted torque and safety factor, the allowed minimum pull-out torque of the radial Halbach PMC is 25N·m. We can see that the PMC initial design cannot meet the needs of practical applications. Since the analytical method and 2-D FEA are proved to be not accurate enough, the analytical solution will only be used to analyze the effect of PMC parameters. For better accuracy, an optimization procedure based on 3-D FEA is established to obtain optimized PMCs with larger pull-out torque with minimal PM material mass.

4. Description of the Optimization Problem

4.1. Objective Function. The structure optimization of PMCs can be achieved by defining the objective function, optimization variables, and constraint functions. This optimization problem can be expressed as follows:

$$\min f(\mathbf{x}) \quad \mathbf{x} \in D$$
$$D = \left\{\mathbf{x} \mid g_p(\mathbf{x}) \le 0,\ p = 1, 2, \cdots, q\right\} \tag{13}$$

where $\mathbf{x}$ is the optimization variables vector, $f(\mathbf{x})$ is the objective function, and $g_p(\mathbf{x})$ are constraint functions.

The purpose of this research is to design a radial Halbach PMC with maximal pull-out torque and minimal PM material mass at the same external dimensions (R_{1o}=27mm, L_a=50mm), and this is a multiple-objective optimization problem. For the practical requirement, a judgment criterion is proposed as the objective function in this research.

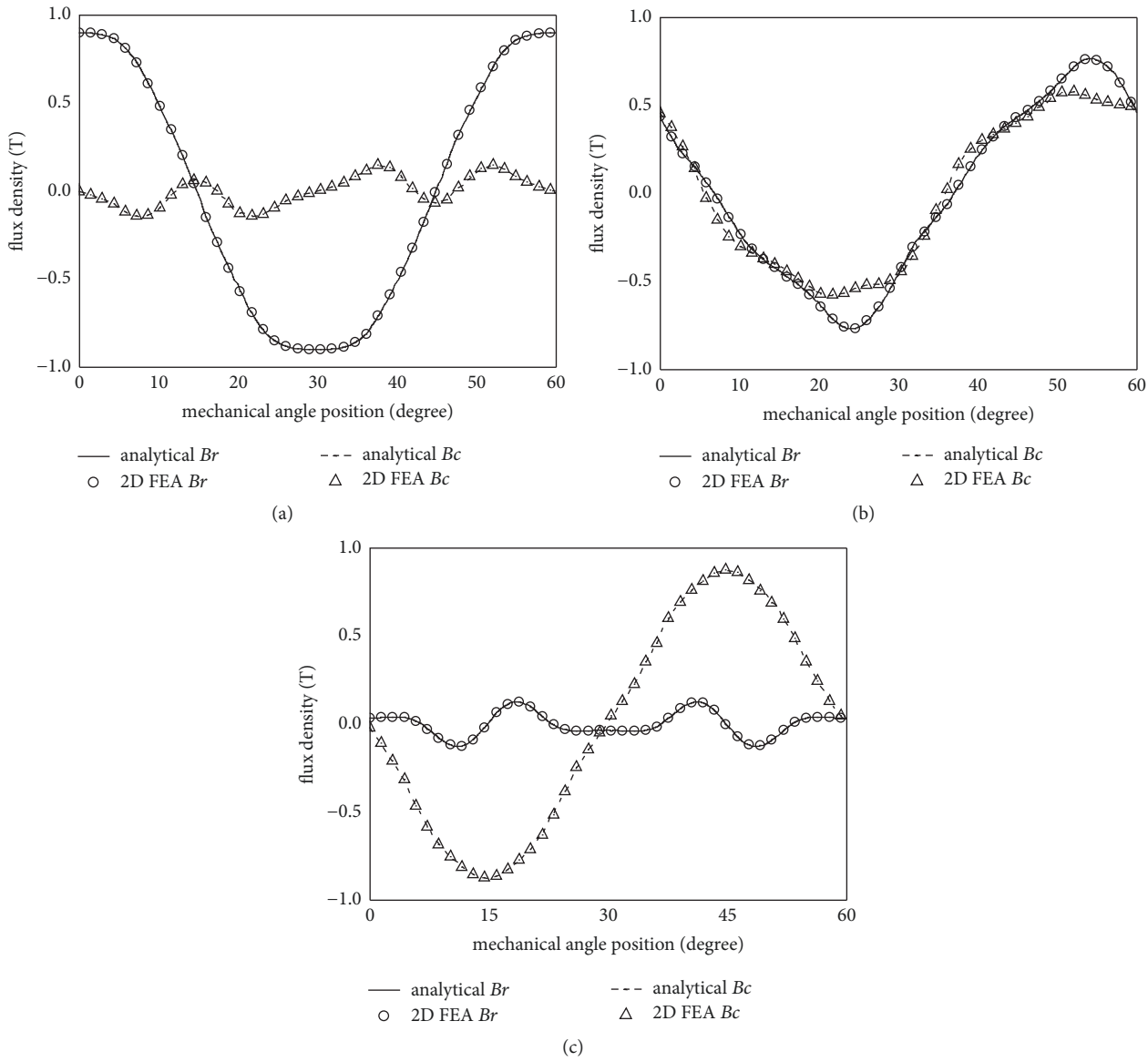

Figure 4: Analytical solutions of radial and circumferential flux density compared with 2-D FEA results in air region r=22.4mm, (a) δ=0°, (b) δ=15°, (c) δ=30°.

The pull-out torque and the PM material mass of PMCs have different units, so dimensionless method is used to construct the objective function. Because maximizing the pull-out torque is a maximal optimization problem, and minimizing the PM material mass is a minimal optimization problem, the objective function can be expressed as follows:

$$f(x) = \omega_1 \cdot \frac{average(T_{\max})}{T_{\max}} + \omega_2 \cdot \frac{m}{average(m)} \tag{14}$$

where the weight coefficients ω_1 and ω_2 (ω_1+ω_2=1) represent the important degree of the pull-out torque and the PM material mass, respectively, and their value can be adjusted according to different application requirements. In this paper, ω_1 is set to 0.7, and ω_2 is set to 0.3. The total PM material mass of the inner and outer rotor can be obtained from

$$\begin{aligned} m = \rho\pi L_a \left[h_{m1}\left(2R_{1o} - h_{m1}\right)\right. \\ \left. + \alpha h_{m3}\left(2R_{1o} - 2h_{m1} - 2g - h_{m3}\right)\right] \end{aligned} \tag{15}$$

In this way, the multiple-objective optimization problem is successfully translated into a solvable single objective optimization. This conversion will make it more efficient to implement the optimal design.

4.2. Optimization Variables. The analytical method is used to analyze the effect of PMC parameters on the magnetic torque. As can been seen from the analytical solution, the outer and inner PM thickness, segment arc coefficient, pole-arc coefficient, and pole pair number will affect the pull-out

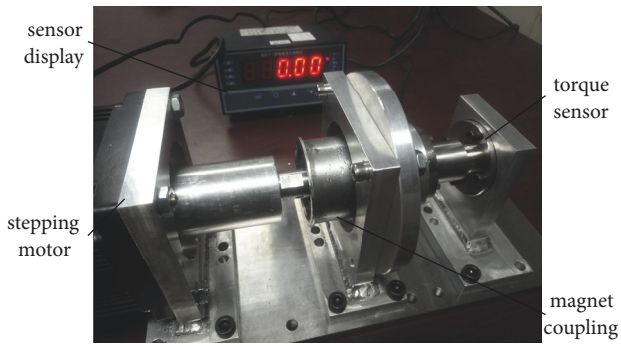

Figure 5: Photograph of the experimental apparatus for measuring the magnetic torque.

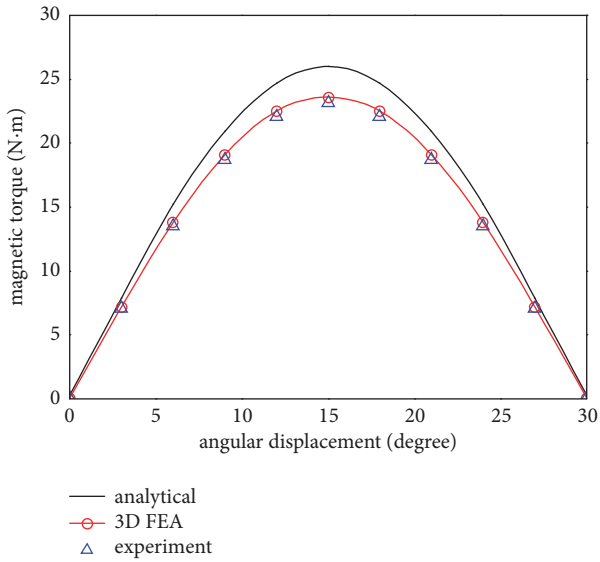

Figure 6: Calculated and experimental results of the magnetic torque with changes of angular displacement.

torque of PMCs. The range of these variables in this research can be listed as follows:

$$\begin{aligned} 2mm \le h_{m1} \le 4mm \\ 3mm \le h_{m3} \le 5mm \\ 0.5 \le \alpha_{rp} \le 0.9 \\ 0.7 \le \alpha \le 1 \\ 3 \le p \le 8, \quad p \in \mathrm{N}* \end{aligned} \tag{16}$$

It should be noted that the pole pair number can only be taken as a positive integer, which means the pole pair number is difficult to be optimized. The analytical and 3-D FEA results of the pull-out torque with changes of pole pair numbers are shown in Figure 7. We can see that pole pair number has great influence on the pull-out torque. For the radial Halbach PMC in this research, when pole pair number is 6, the pull-out torque reaches its maximum. Therefore, the pole pair number will be regarded as a constant in the optimization procedure.

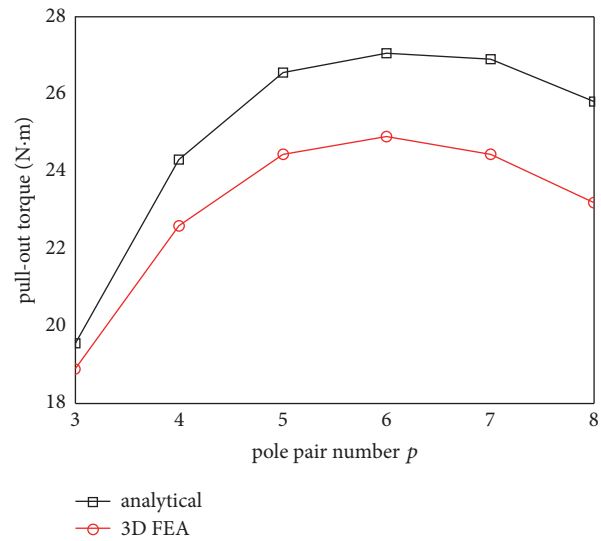

Figure 7: Pull-out torque with changes of pole pair numbers, when h_{m1}=3mm, h_{m2}=4mm, α_{rp}=0.7, α=0.85.

The final optimization variables including four parameters are as follows.

$$\mathbf{x} = \left(h_{m1}, h_{m3}, \alpha_{rp}, \alpha\right) \tag{17}$$

4.3. Optimization Procedure. For the nonlinear function of pull-out torque, it is difficult to accurately find the extremum only through a certain number of discrete input data and output data. The nonlinear fitting ability of BPNN and the nonlinear optimization ability of GA can be used to find the extremum. BPNN and GA have been used at some of the nonlinear data to find the optimal solution [17, 18], and this method proved to be feasible. This paper establishes an optimization procedure based on the combination of 3-D FEA, BPNN, and GA. The optimization procedure is to obtain the pull-out torque of the samples by 3-D FEA and use BPNN to establish the prediction model between the optimization variables and pull-out torque. Then GA is applied to solve the optimization model, and the solution of the optimal problem can be obtained. The optimization procedure of BPNN predication model and the numerical optimization with GA is shown in Figure 8.

5. BPNN Prediction Model

BPNN is a multilayer feedforward network trained based on error back propagation algorithm, and it has a great learning ability in training and mapping the relations between inputs and outputs. BPNN can be accepted as an alternative to providing solutions to complex and ambiguous problems [19]. This paper adopts BPNN to construct the prediction model of the pull-out torque.

The topology of the BPNN in this paper is shown in Figure 9. Each node of the structure represents a neuron. The network takes four optimization variables as the input neurons and takes the pull-out torque as the output neuron, so the structure has four input layer nodes and one output

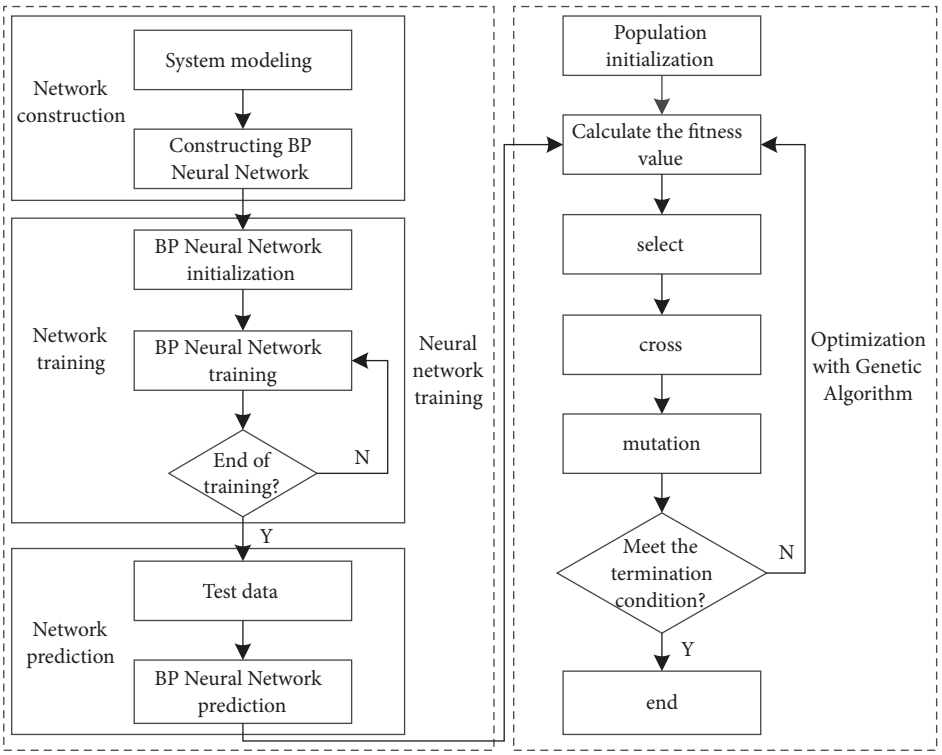

Figure 8: The optimization procedure of BPNN and GA.

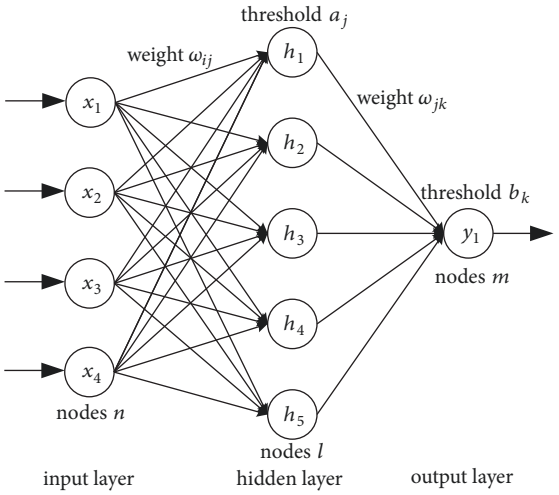

Figure 9: The topology of the BPNN.

layer node. After several attempts and contrasts, the number of hidden layer nodes is selected as 5. The weights and thresholds of neural network are adjusted according to the error during the training, so that the predicted output of the network is constantly approximating the expected output.

A certain number of samples are necessary in the network training process, and they should be able to describe the entire design space. Latin hypercube sampling can generate a certain number of near-random samples of design variables from a multidimensional distribution. This sampling method is frequently used to construct computer experiments. In order to ensure the prediction model is accurate enough, 40 samples are randomly selected from the optimization variable ranges using the Latin hypercube sampling method in this research. The pull-out torque of the samples is calculated by 3-D FEA. The samples and corresponding responses (pull-out torque) are shown in Table 3.

In order to obtain a better training effect, the sample data should be normalized in $[-1\ \ 1]$ before training. MATLAB neural network toolbox is used to train the BPNN. We set the target error of the network to 0.000004, the learning rate to 0.1, and the number of training steps to 100. All the iteration processes of the BPNN have mean square errors (*MSE*), as shown in (18). We set *MSE* as a performance function of the training. In addition, the average accuracy of the prediction (R) is defined as (19). R represents the goodness of fit and is used to measure the correlation between predicted output data and training sample data. The closer R is to 1, the more predictable the training network is.

$$MSE = \frac{1}{mp}\sum_{p=1}^{p}\sum_{j=1}^{m}\left(\widehat{y}_{pj} - y_{pj}\right)^2 \tag{18}$$

$$R = \frac{1}{p}\sum_{i=1}^{p}\frac{y_{pj}}{\widehat{y}_{pj}} \tag{19}$$

According to the above settings, the training of BPNN is carried out until the training network meets the intended

Table 3: 40 samples and corresponding responses.

No.	h_{m1}	h_{m3}	α_{rp}	α	$T_{\max}$	No.	h_{m1}	h_{m3}	α_{rp}	α	$T_{\max}$
1	2.85	4.88	0.719	0.953	25.65	21	2.05	3.22	0.829	0.901	21
2	3.08	4.51	0.501	0.707	21.75	22	3.14	3.19	0.813	0.988	24.7
3	3.54	4.04	0.584	0.863	25.35	23	2.74	4.17	0.728	0.816	24.15
4	2.42	4.72	0.706	0.727	22.35	24	3.86	4.31	0.536	0.781	24.55
5	2.57	3.38	0.546	0.835	21.4	25	3.98	4.28	0.878	0.932	26.35
6	2.85	3.34	0.767	0.903	24.15	26	2.53	4.59	0.688	0.756	22.9
7	3.17	4.69	0.836	0.912	26.2	27	3.69	4.07	0.85	0.714	24.35
8	3.57	3.74	0.554	0.775	23.85	28	3.23	3.88	0.623	0.968	25.5
9	2.66	5	0.841	0.811	24.45	29	3.65	3.58	0.807	0.787	24.9
10	2.22	3.29	0.798	0.854	21.65	30	2.37	4.22	0.785	0.805	22.95
11	2.17	4.1	0.642	0.765	20.85	31	3.42	4.92	0.57	0.879	25.65
12	3.34	3.45	0.867	0.936	25.2	32	2.97	3.1	0.897	0.797	22.9
13	2.11	4.4	0.739	0.74	1.2	33	2.91	3.5	0.666	0.84	23.8
14	3.02	4.81	0.671	0.972	25.9	34	3.75	3.61	0.593	0.943	25.7
15	3.82	3.75	0.76	0.98	26.5	35	2.47	4.77	0.653	0.921	23.85
16	2.34	4.47	0.74	0.888	23.5	36	3.91	3.43	0.579	0.827	24.75
17	3.76	4.37	0.618	0.734	24.65	37	2.02	3.94	0.514	0.715	17.85
18	2.29	3.13	0.638	0.958	21.35	38	2.64	3.67	0.528	0.994	22.5
19	3.25	3.05	0.77	0.887	24.4	39	3.47	4.62	0.881	0.846	25.85
20	2.77	3.96	0.695	0.869	24.4	40	3.36	3.84	0.609	0.749	23.85

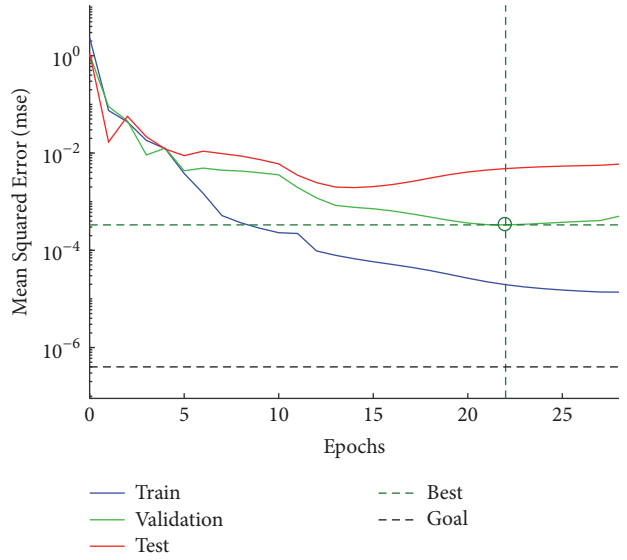

Figure 10: The validation performance of the BPNN.

target. Figure 10 shows that the validation performance of the trained neural network is closest to the target error at epoch 22. Figure 11 shows the regression analysis of the BPNN. As can be seen from Figure 11, the training set, the validation set, and the test set of R are all close to 1. It indicates that the constructed BPNN has high prediction accuracy.

10 samples are also taken from the variable ranges with the Latin hypercube sampling method to test the prediction model, as shown in Table 4, and the corresponding pull-out torque is calculated by 3-D FEA. Figure 12 shows the comparison of the neural network predicted output with expected output of the test samples. It can be seen that the training network is close to the date, the maximal relative error between the predicted output and expected output is only about 0.9%, and this error is acceptable in engineering. The prediction model of BPNN is relatively accurate to be used in the optimization procedure of PMCs.

Table 4: 10 samples used to test the trained BPNN.

No.	h_{m1}	h_{m3}	α_{rp}	α	$T_{\max}$
1	3.64	3.58	0.564	0.791	24.1
2	2.22	3.31	0.746	0.925	21.85
3	3.38	4.89	0.782	0.996	26.85
4	3.98	3.1	0.687	0.737	23.75
5	3.2	4.46	0.524	0.845	24.2
6	2.97	4.19	0.589	0.784	23.55
7	3.41	4.8	0.636	0.719	24.35
8	2.11	3.9	0.725	0.94	22
9	2.8	4.4	0.842	0.891	25.15
10	2.5	3.69	0.865	0.877	23.45

6. Optimization Using GA

GA is a computational model of the biological evolution process of the simulation genetic mechanism. It is a frequently used method to search the optimal solution for the feasible solution of the problem [20]. In this paper, GA is applied to solve the optimization problem to obtain the design variables with maximal pull-out torque and minimal PM material mass.

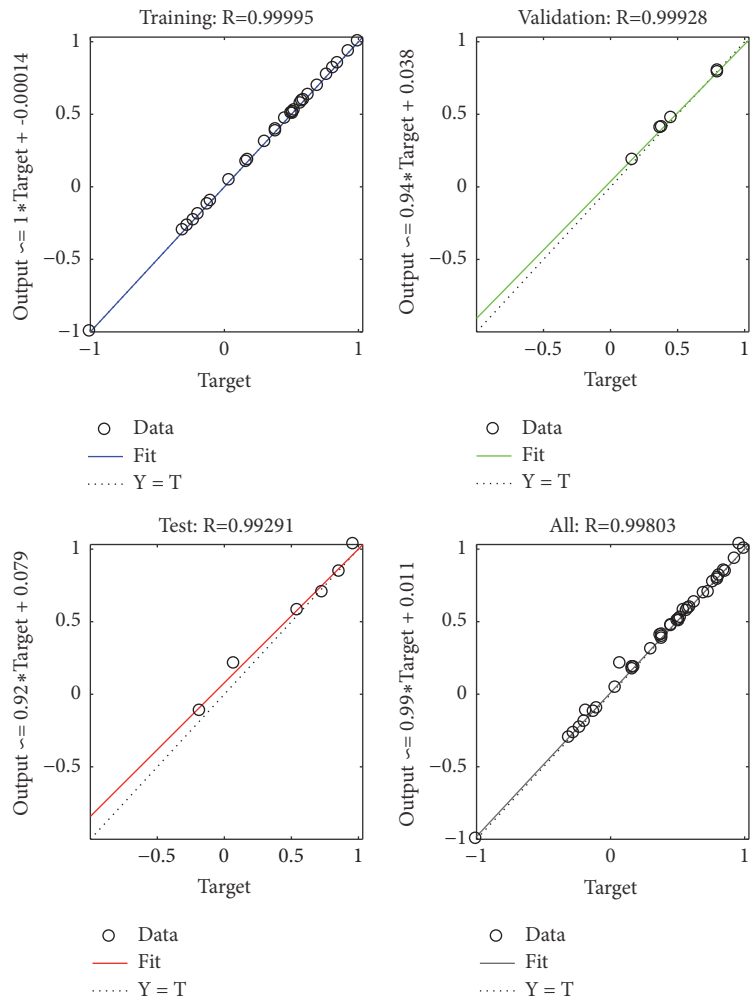

Figure 11: The regression analysis of the BPNN.

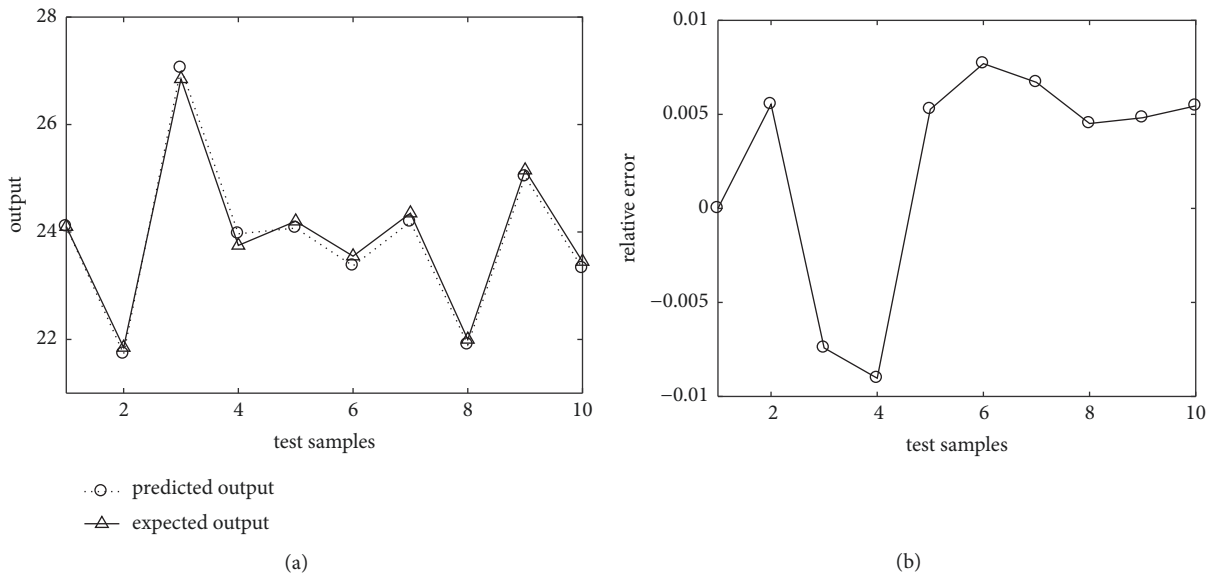

Figure 12: Comparison of predicted output and expected output.

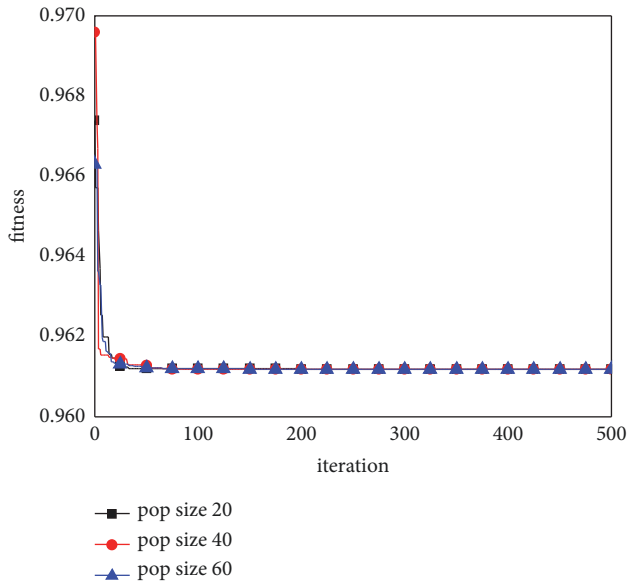

Figure 13: Fitness with changes of iterations under three different population sizes.

Table 5: Comparison of optimized results and initial design.

Parameters	Initial design	Optimized results
h_{m1}/mm	3	3.31
h_{m3}/mm	4	3.90
α_{rp}	0.5	0.782
α	1	0.856
T_{max}/N·m	23.6	25.7
m/g	357.4	343.5

This multiobjective optimization problems are solved by the following GA parameters: number of iterations-500, crossover probability-0.7, and mutation probability-0.1. Three different population sizes of the GA have been executed and compared. The fitness varies with the number of iterations under different population sizes as shown in Figure 13. The convergent fitness is all 0.9611918, and the error is less than 10^{-7}. When the population size is 20, after several executions of the optimization procedure, the GA converges to an identical solution. The same applies to the case of population sizes 40 and 60. Furthermore the optimal solutions under population sizes of 20, 40, and 60 are the same.

3-D FEA is used to analyze the optimized scheme, and the optimized results are as depicted in Table 5. The pull-out torque of the optimized scheme is 8.90% larger than that of the initial design, and the PM material mass is 3.89% less than that of the initial design at the same time. Therefore, this optimized scheme can be well suited to the needs of practical applications. 2-D FEA is also used to evaluate the optimized scheme. The flux line distribution of the optimized scheme is plotted in Figure 14 and is compared with that of the initial design. From the results of 3-D FEA, the magnetic density vector of the optimized scheme and the initial design are exhibited and compared in Figure 15. As we can see, the optimized scheme makes better use of the outer rotor core, and the flux density in the inner rotor core, in the inner PMs, and in the outer PMs will decrease slightly. The magnetic field distribution of the optimized scheme is more reasonable.

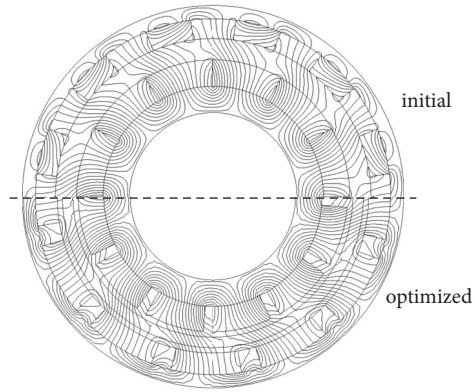

Figure 14: Magnetic flux line distribution of the optimized scheme and the initial design.

7. Conclusions

In this paper, a two-segment Halbach array is adopted in the outer PMs of the radial PMC, and the segment arc coefficient can be adjusted to get larger magnetic torque. Based on analytical magnetic field and Maxwell stress tensor, the general analytical solutions of radial Halbach PMCs are obtained. The analytical solution of magnetic field is in good agreement with the 2-D FEA results. In addition, an initial PMC prototype has been fabricated. The pull-out torque calculated with the analytical method is 11.6% larger than the experimental result, and the 3-D FEA result is close to the experimental result. Then, this paper establishes an optimization procedure for PMCs based on the combination of 3-D FEA, BPNN, and GA. BPNN is used to establish the prediction model of pull-out torque based on 40 samples from Latin hypercube sampling. The test of the BPNN prediction model shows the maximal relative error between the predicted output and expected output is only about 0.9%. Finally, GA is applied to achieve the optimized scheme of the radial Halbach PMC, and the 3-D FEA results show that the pull-out torque of the optimized scheme is 8.90% larger than that of the initial design; meanwhile, the PM material mass is 3.89% less than that of the initial design.

Data Availability

The data used to support the findings of this study are available from the corresponding author upon request.

Conflicts of Interest

The authors declare that there are no conflicts of interest regarding the publication of this paper.

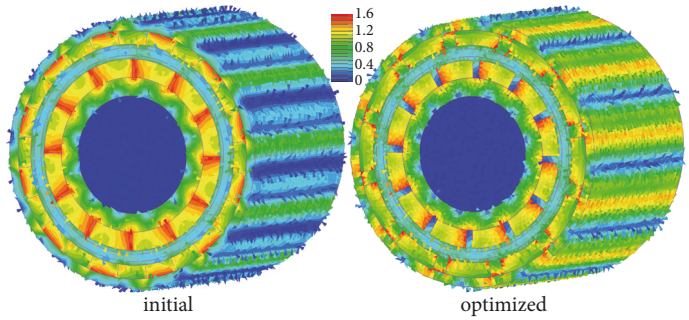

Figure 15: Magnetic density vector of the optimized scheme and the initial design.

Acknowledgments

This work was supported by the National Science Foundation of China (Grant No. 51479170 and No. 11502210) and National Key R&D Plan of China (Grant No. 2016YFC0301300).

References

[1] Q. C. Tan, D. Xin, W. Li, and H. Meng, "Study on Transmitting Torque and Synchronism of Magnet Couplings," *Proceedings of the Institution of Mechanical Engineers, Part C: Journal of Mechanical Engineering Science*, vol. 206, no. 6, pp. 381–384, 1992.

[2] V. V. Fufaev and A. Y. Krasilnikov, "Torque of a cylindrical magnetic coupling," *Russian Electrical Engineering*, vol. 65, no. 8, pp. 51–53, 1994.

[3] J. F. Charpentier and G. Lemarquand, "Study of permanent-magnet couplings with progressive magnetization using an analytical formulation," *IEEE Transactions on Magnetics*, vol. 35, no. 5, pp. 4206–4217, 1999.

[4] J. F. Charpentier and G. Lemarquand, "Calculation of ironless permanent magnet couplings using semi-numerical magnetic pole theory method," *COMPEL - The International Journal for Computation and Mathematics in Electrical and Electronic Engineering*, vol. 20, no. 1-4, pp. 72–89, 2001.

[5] S. M. Huang and C. K. Sung, "Analytical analysis of magnetic couplings with parallelepiped magnets," *Journal of Magnetism and Magnetic Materials*, vol. 239, no. 1-3, pp. 614–616, 2002.

[6] R. Ravaud and G. Lemarquand, "Comparison of the coulombian and amperian current models for calculating the magnetic field produced by radially magnetized arc-shaped permanent magnets," *Progress in Electromagnetics Research*, vol. 95, pp. 309–327, 2009.

[7] R. Ravaud, G. Lemarquand, V. Lemarquand, and C. Depollier, "Torque in permanent magnet couplings: Comparison of uniform and radial magnetization," *Journal of Applied Physics*, vol. 105, no. 5, 2009.

[8] R. Ravaud, V. Lemarquand, and G. Lemarquand, "Analytical design of permanent magnet radial couplings," *IEEE Transactions on Magnetics*, vol. 46, no. 11, pp. 3860–3865, 2010.

[9] E. P. Furlani, "Analysis and optimization of synchronous magnetic couplings," *Journal of Applied Physics*, vol. 79, no. 8, pp. 4692–4694, 1996.

[10] T. Lubin, S. Mezani, and A. Rezzoug, "Simple analytical expressions for the force and torque of axial magnetic couplings," *IEEE Transactions on Energy Conversion*, vol. 27, no. 2, pp. 536–546, 2012.

[11] H.-B. Kang and J.-Y. Choi, "Parametric analysis and experimental testing of radial flux type synchronous permanent magnet coupling based on analytical torque calculations," *Journal of Electrical Engineering & Technology*, vol. 9, no. 3, pp. 926–931, 2014.

[12] C.-W. Kim and J.-Y. Choi, "Parametric analysis of tubular-type linear magnetic couplings with halbach array magnetized permanent magnet by using analytical force calculation," *Journal of Magnetics*, vol. 21, no. 1, pp. 110–114, 2016.

[13] S. Hogberg, B. B. Jensen, and F. B. Bendixen, "Design and demonstration of a test-rig for static performance-studies of permanent magnet couplings," *IEEE Transactions on Magnetics*, vol. 49, no. 12, pp. 5664–5670, 2013.

[14] H.-B. Kang, J.-Y. Choi, H.-W. Cho, and J.-H. Kim, "Comparative study of torque analysis for synchronous permanent magnet coupling with parallel and halbach magnetized magnets based on analytical field calculations," *IEEE Transactions on Magnetics*, vol. 50, no. 11, 2014.

[15] W. Y. Lin, L. P. Kuan, W. Jun, and D. Han, "Near-optimal design and 3-D finite element analysis of multiple sets of radial magnetic couplings," *IEEE Transactions on Magnetics*, vol. 44, no. 12, pp. 4747–4753, 2008.

[16] W. Wu, H. Lovatt, and J. Dunlop, "Analysis and design optimisation of magnetic couplings using 3D finite element modelling," *IEEE Transactions on Magnetics*, vol. 33, no. 5, pp. 4083–4094.

[17] F. Yin, H. Mao, and L. Hua, "A hybrid of back propagation neural network and genetic algorithm for optimization of injection molding process parameters," *Materials & Design*, vol. 32, no. 6, pp. 3457–3464, 2011.

[18] K. Hu, A. Song, M. Xia, X. Ye, and Y. Dou, "An adaptive filtering algorithm based on genetic algorithm-backpropagation network," *Mathematical Problems in Engineering*, vol. 2013, Article ID 573941, 8 pages, 2013.

[19] J. Li, J. H. Cheng, J. Y. Shi, and F. Huang, "Brief introduction of back propagation (BP) neural network algorithm and its improvement," in *Advances in Computer Science and Information Engineering*, D. Jin and S. Lin, Eds., vol. 169, pp. 553–558, Springer, Berlin, Germany, 2012.

[20] C. R. Houck, J. Joines, and M. G. Kay, "A genetic algorithm for function optimization: a matlab implementation," *NCSU-IE TR*, vol. 95, no. 9, 1995.

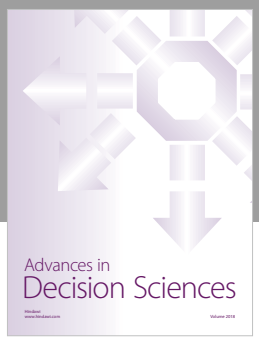

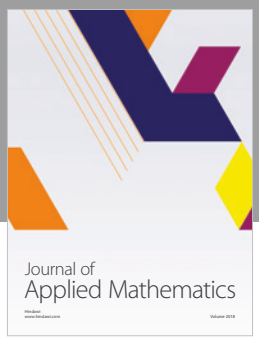

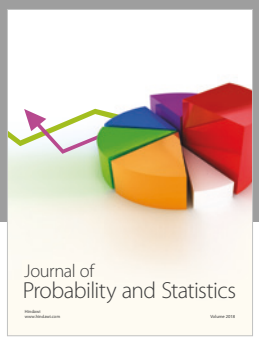

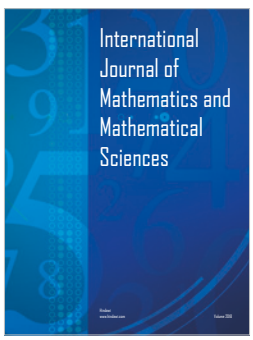

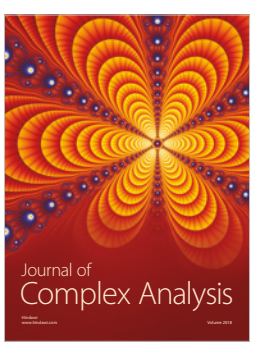

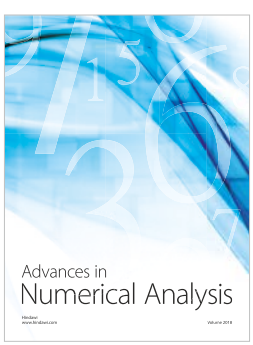

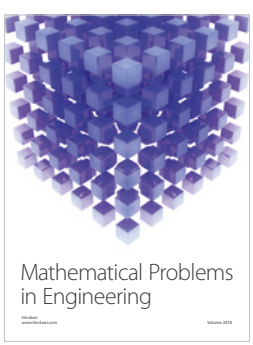

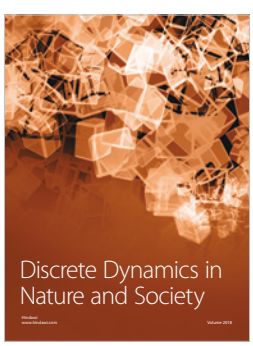

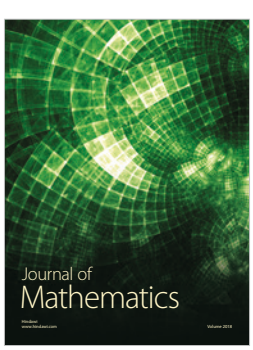

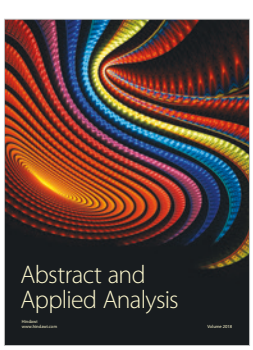

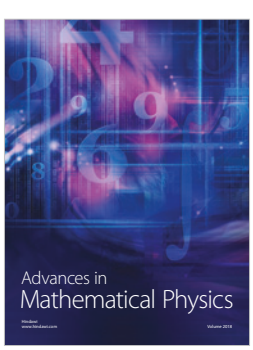

Hindawi

Submit your manuscripts at
www.hindawi.com